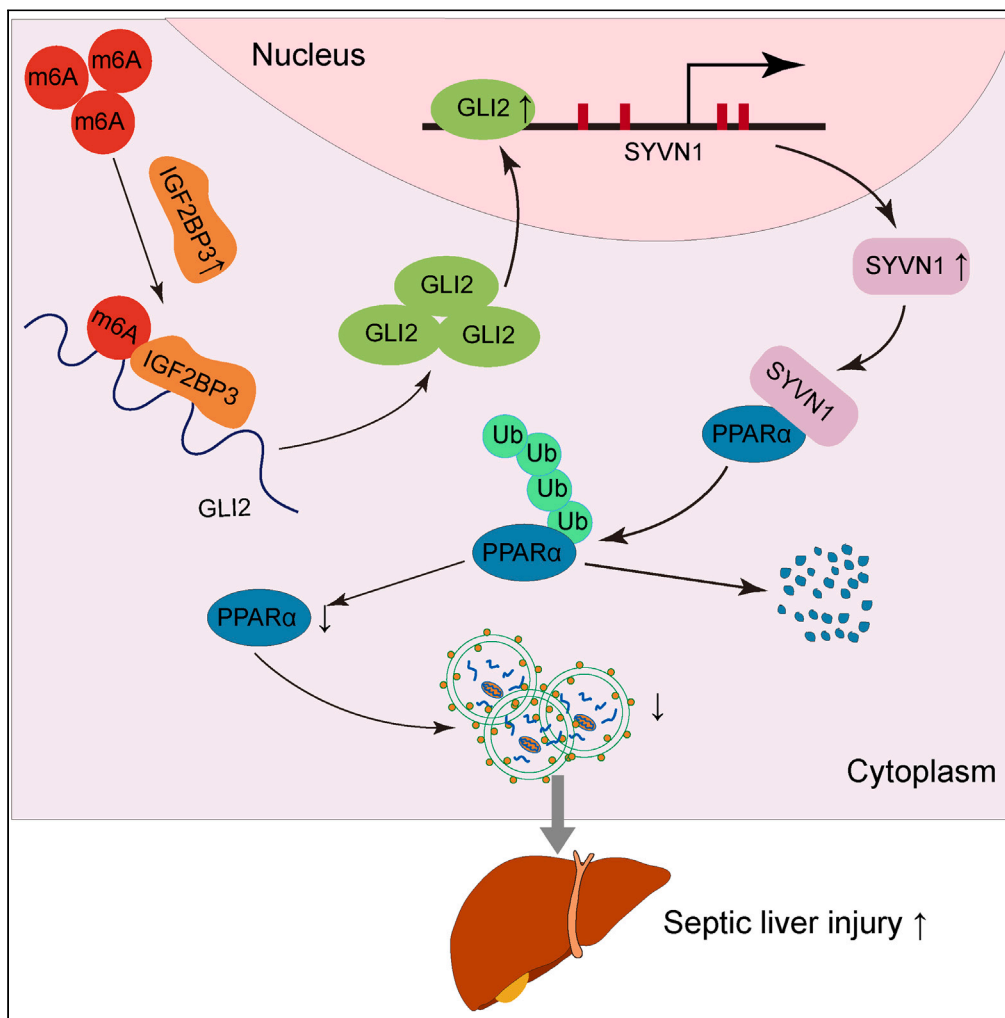


Article

IGF2BP3 modified GLI2 transcriptionally regulates SYVN1 and facilitates sepsis liver injury through autophagy



Chuanzheng Sun,
Min Gao, Haotian
Hu, ..., Xiaoxue
Cao, Runbang
Zhang, Huaizheng
Liu

lh33385@csu.edu.cn

Highlights

Knockdown of GLI2,
SYVN1, or IGF2BP3
promoted
PPARα-mediated
autophagy

GLI2 promoted the
ubiquitination degradation
of PPARα via SYVN1

IGF2BP3 recognized the
m6A site of GLI2 and
increased its mRNA
stability

IGF2BP3/SYVN1 silencing
promoted autophagy and
improved septic liver injury
in vivo

Sun et al., iScience 27, 109870
June 21, 2024 © 2024 Published
by Elsevier Inc.
[https://doi.org/10.1016/
j.isci.2024.109870](https://doi.org/10.1016/j.isci.2024.109870)



Article

IGF2BP3 modified GLI2 transcriptionally regulates SYVN1 and facilitates sepsis liver injury through autophagy

Chuanzheng Sun,¹ Min Gao,² Haotian Hu,¹ Jing Qi,¹ Yishu Tang,¹ Xiaoxue Cao,¹ Runbang Zhang,¹ and Huaizheng Liu^{1,3,*}

SUMMARY

Autophagy enhancement in septic liver injury can play a protective role. Nevertheless, the mechanism of autophagy-mediated septic liver injury needs further investigation. Our study demonstrated that in septic condition, GLI Family Zinc Finger 2 (GLI2) was elevated, whereas peroxisome-proliferator-activated receptor α (PPAR α) was downregulated. Suppressing GLI2 or synovialapoptosis inhibitor 1 (SYVN1) in LPS-exposed cells increased PPAR α levels, enhanced cell viability and autophagy, while inhibiting apoptosis. LPS enhanced the GLI2-SYVN1 promoter binding. SYVN1 fostered ubiquitin-mediated degradation of PPAR α . IGF2BP3 stabilized GLI2 mRNA by targeting its m⁶A site. Silencing IGF2BP3 led to decreased GLI2 and SYVN1 but increased PPAR α levels, promoting cell survival and autophagy, while repressing apoptosis. This was counteracted by SYVN1 overexpression. In cecal ligation and puncture mice, IGF2BP3, SYVN1, or GLI2 knockdown ameliorated liver damage and augmented autophagy. In summary, IGF2BP3 enhanced GLI2 stability, overexpressed GLI2 subsequent promoted SYVN1 levels by interacting with its promoter, leading to ubiquitinated degradation of PPAR α , thereby inhibiting PPAR α -mediated autophagy and then exacerbating liver injury in sepsis.

INTRODUCTION

Sepsis is a critical medical condition associated with a high mortality rate and complex clinical challenges.¹ Liver injury has been recognized as an early indicator of sepsis and an independent and considerable risk factor in poor prognosis of sepsis patients.^{2,3} Therefore, developing therapies to improve liver injury is essential for reducing sepsis-related mortality. Previous studies have emphasized the vital role of autophagy in improving liver injury caused by sepsis. For instance, carbamazepine (CBZ), an autophagy enhancer, was suggested to alleviate liver injury in mice with cecal ligation and puncture (CLP)-sepsis.⁴ However, the mechanism of autophagy-mediated liver injury in sepsis remains poorly understood.

Peroxisome-proliferator-activated receptor α (PPAR α) has been demonstrated to be an important factor regulating autophagy in the clearance of amyloid beta (A β).⁵ Moreover, PPAR α has been linked to the inhibition of cancer cell growth by enhancing autophagy.⁶ PPAR α transcriptionally activates transcription factor EB (TFEB), the master autophagy gene transcription factor that can enhance lysosome biogenesis and autophagy.⁷ We therefore hypothesized that PPAR α -mediated autophagy may affect septic liver injury. Interestingly, decreased PPAR α expression has been observed in septic mice, and the increase of PPAR α levels and activity improved mortality in CLP-induced peritonitis sepsis mouse models.⁸ However, the precise role of PPAR α in sepsis and its potential connection to autophagy induction require further investigation.

Hedgehog (Hh) signaling pathway has proved to modulate the regeneration and repair responses to liver injury.^{9–11} Among the key effectors of the Hh pathway, GLI Family Zinc Finger 2 (GLI2) has been found to modulate Hh pathway activity by increasing the expression of its inhibitors.¹² The inhibition of GLI2 could ameliorate CCl₄-induced liver fibrosis by reducing Hh activity.¹³ However, the role of GLI2 in septic liver injury remains to be explored. Insulin-like growth factor 2 mRNA binding protein 3 (IGF2BP3) has indicated to be pivotal for recognizing N⁶-methyladenosine (m⁶A) modification and regulate mRNA stabilization and translation.^{14,15} m⁶A modifications are well-known modifications of eukaryotic mRNAs, which affect key processes of mRNA metabolism, including mRNA localization, splicing, translation and degradation, profoundly regulating several physiological processes and disease pathogenesis.^{16,17} Interestingly, m⁶A RNA methylation has been linked to the heterogeneity of sepsis,¹⁸ and increased expression of IGF2BP3 was observed in sepsis.¹⁹ Herein, the m⁶A modification sites in

¹Department of Emergency, The Third Xiangya Hospital, Central South University, Changsha 410013, Hunan Province, P.R. China

²Department of Critical Care Medicine, The Third Xiangya Hospital, Central South University, Changsha 410013, Hunan Province, P.R. China

³Lead contact

*Correspondence: lh3385@csu.edu.cn
<https://doi.org/10.1016/j.isci.2024.109870>



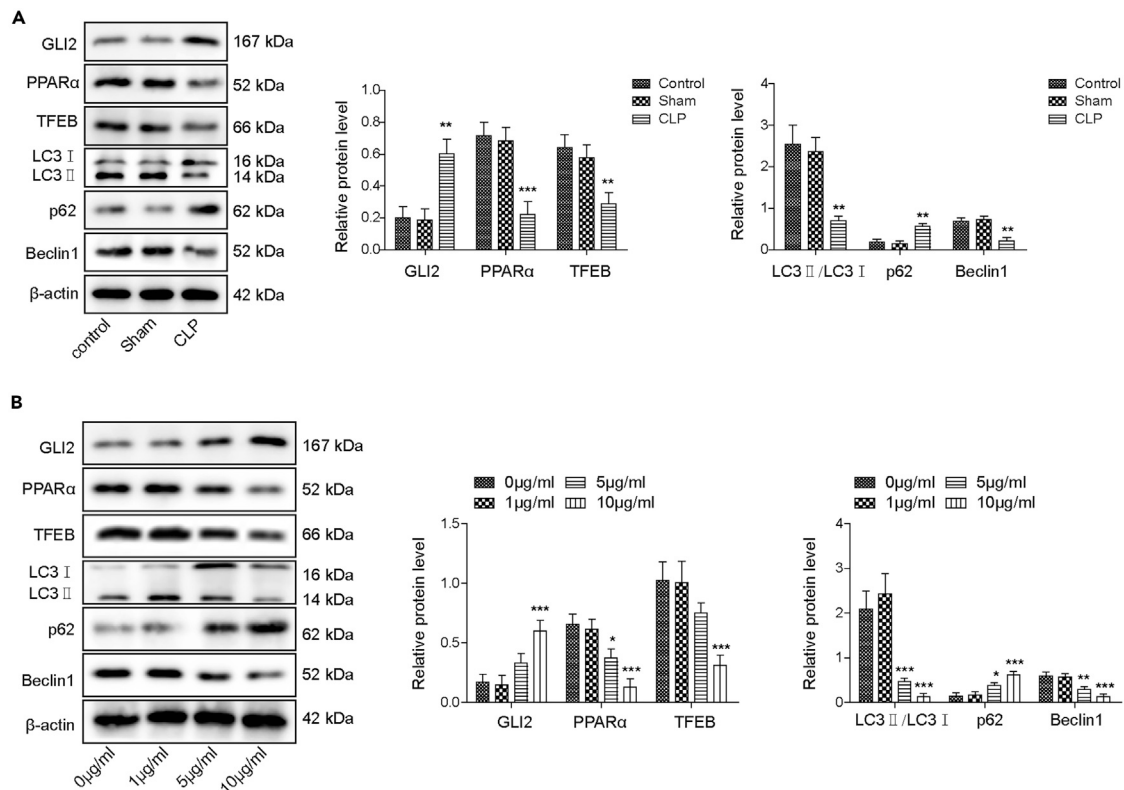


Figure 1. GLI2 and PPAR α were upregulated in liver tissues of septic mice, while the levels of autophagy-related proteins were decreased

Septic mouse models were established by cecal ligation and puncture (CLP) surgery ($n = 5$ for each group).

(A) The expression of GLI2, PPAR α , and autophagy-related proteins (TFEB, LC3-II/I, p62, and Beclin-1) in liver tissues of septic mice was measured by Western blotting. Blots for β -actin served as loading controls. Primary hepatocytes were incubated with LPS for 8 h at different dosages (0, 1, 5, or 10 μ g/ml).

(B) The expression of GLI2, PPAR α , and autophagy-related proteins in LPS-induced hepatocytes was measured by Western blotting. β -actin served as loading controls. Mean \pm standard deviation (SD), $n = 3$, $*p < 0.05$, $**p < 0.01$, $***p < 0.001$. Statistical analysis was carried out by a Student's t test or a one-way ANOVA.

GLI2 transcripts, as well as the binding sites between IGF2BP3 and GLI2 mRNA were predicted. We therefore hypothesized that IGF2BP3 recognized GLI2 m⁶A sites and regulated its stability.

Of note, E3 ubiquitin ligase synovial apoptosis inhibitor 1 (SYVN1), an E3 ubiquitin ligase involved in endoplasmic reticulum-associated degradation,²⁰ has shown differential expression in CLP-induced septic mouse model.²¹ Herein, SYVN1 was predicted to be one of potential specific E3 ligases of PPAR α . Thus, we proposed the hypothesis that IGF2BP3 enhanced the stability of GLI2 by recognizing GLI2 m⁶A sites and subsequent transcriptional upregulation of SYVN1, thereby promoting ubiquitination degradation of PPAR α , leading to a corresponding decrease in PPAR α -mediated autophagy, ultimately contributing to septic liver injury.

RESULTS

GLI2 was upregulated in both liver tissues of septic mice and primary hepatocytes induced by LPS, while PPAR α s exhibited downregulation

CLP surgery was performed to establish septic mouse models. Compared to the Sham group, mice underwent CLP had a lower survival rate (Figure S1A). Moreover, mice showed liver injury with modest areas of necrosis and sinusoid congestion at histological examination after CLP surgery (Figure S1B). In the liver tissues of septic mice, there was a decreased expression of the autophagy marker protein LC3B (Figure S1C), while alanine transaminase (ALT) and aspartate transaminase (AST) levels in the serum were upregulated (Figure S1D). Besides, we measured GLI2, PPAR α , and autophagy-related proteins (TFEB, LC3-II/I, p62, and Beclin-1) expression in liver tissues of septic mice, and found increased levels of GLI2 and p62, while PPAR α , TFEB, LC3-II/I, and Beclin-1 levels decreased (Figure 1A). In *in vitro* experiments, primary hepatocytes were exposed to different concentration LPS (0, 1, 5, or 10 μ g/ml). LPS treatment reduced the viability of hepatocytes and promoted the mortality in a dose-dependent manner (Figures S1E–1G). Meanwhile, LPS treatment increased GLI2 and p62 levels, while decreasing PPAR α , TFEB, LC3-II/I, and Beclin-1 levels in a dose-dependent manner (Figure 1B). We therefore speculated that differential expression of GLI2 and PPAR α in septic mouse and cell models might be a direction worth exploring.

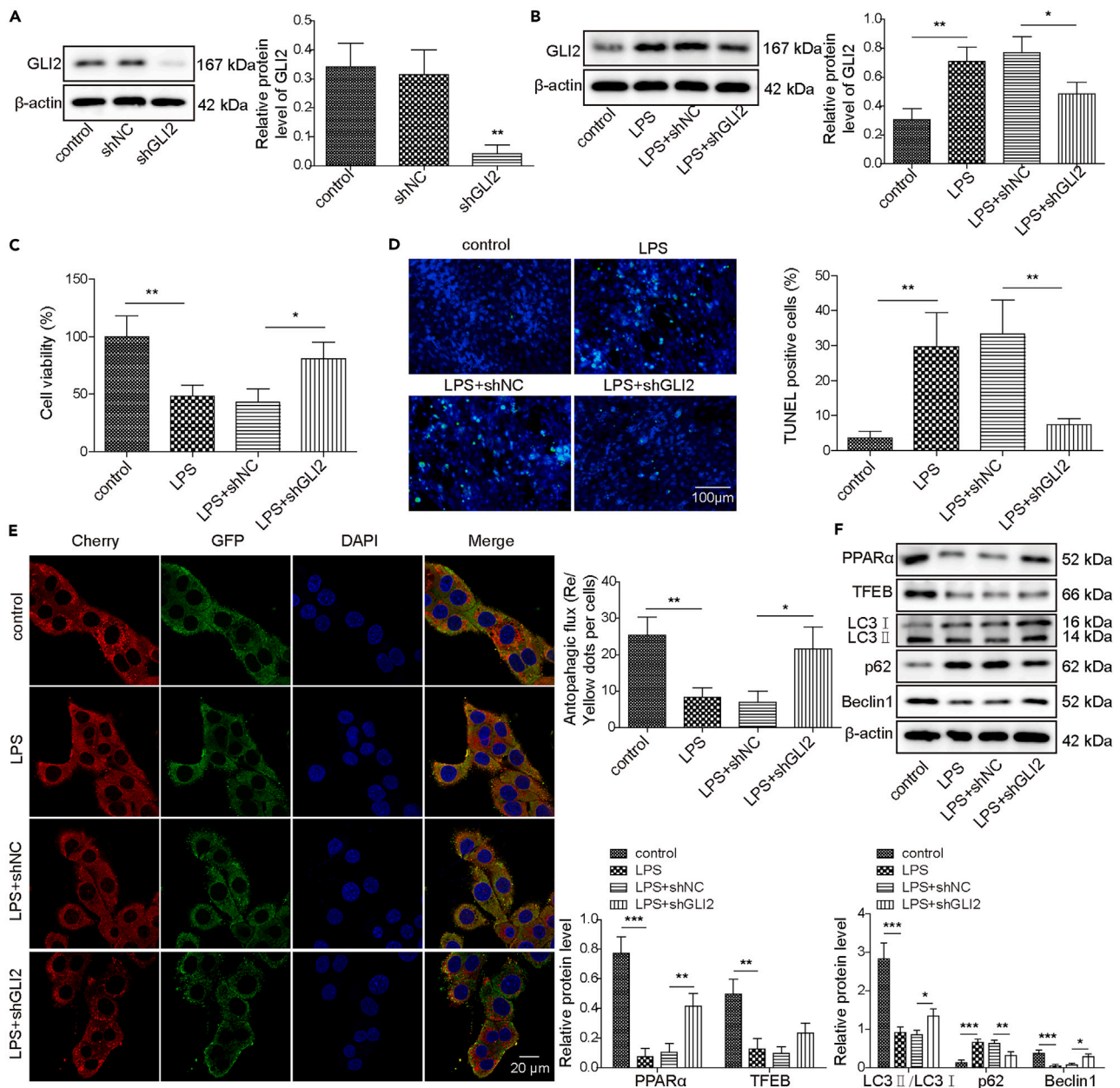


Figure 2. Knockdown of GLI2 promoted autophagy and alleviated LPS-induced septic liver injury *in vitro*

(A) The expression of GLI2 in primary hepatocytes transfected with shGLI2 was measured by western blotting. β -actin served as loading controls. Hepatocytes were treated with LPS (5 μ g/mL), LPS + shNC, and LPS + shGLI2, then (B) GLI2 expression in treated cells were assessed by western blot. β -actin served as loading controls.

(C) The viability of treated hepatocytes was analyzed by MTT.

(D) The mortality of treated hepatocytes was measured by TUNEL staining. Scale bar, 100 μ m.

(E) Representative images of immunofluorescence staining of LC3 in treated hepatocytes. Scale bar, 20 μ m.

(F) Western blotting analysis of PPAR α and autophagy-related proteins expression in treated hepatocytes. β -actin served as loading controls. Mean \pm SD, n = 3,

* p < 0.05, ** p < 0.01, *** p < 0.001. Statistical analysis was carried out by a one-way ANOVA.

Knockdown of GLI2 promoted autophagy and alleviated LPS-induced septic liver injury *in vitro*

To determine the role of GLI2, we transfected shGLI2 plasmids into primary hepatocytes, then induced by LPS. As indicated in Figure 2A, GLI2 was downregulated after transfecting with shGLI2. LPS-driven GLI2 overexpression in hepatocytes was countered when GLI2 was silenced (Figure 2B). Next, the viability and mortality of LPS-treated cells were assessed after transfecting with shGLI2. Knockdown of GLI2 promoted

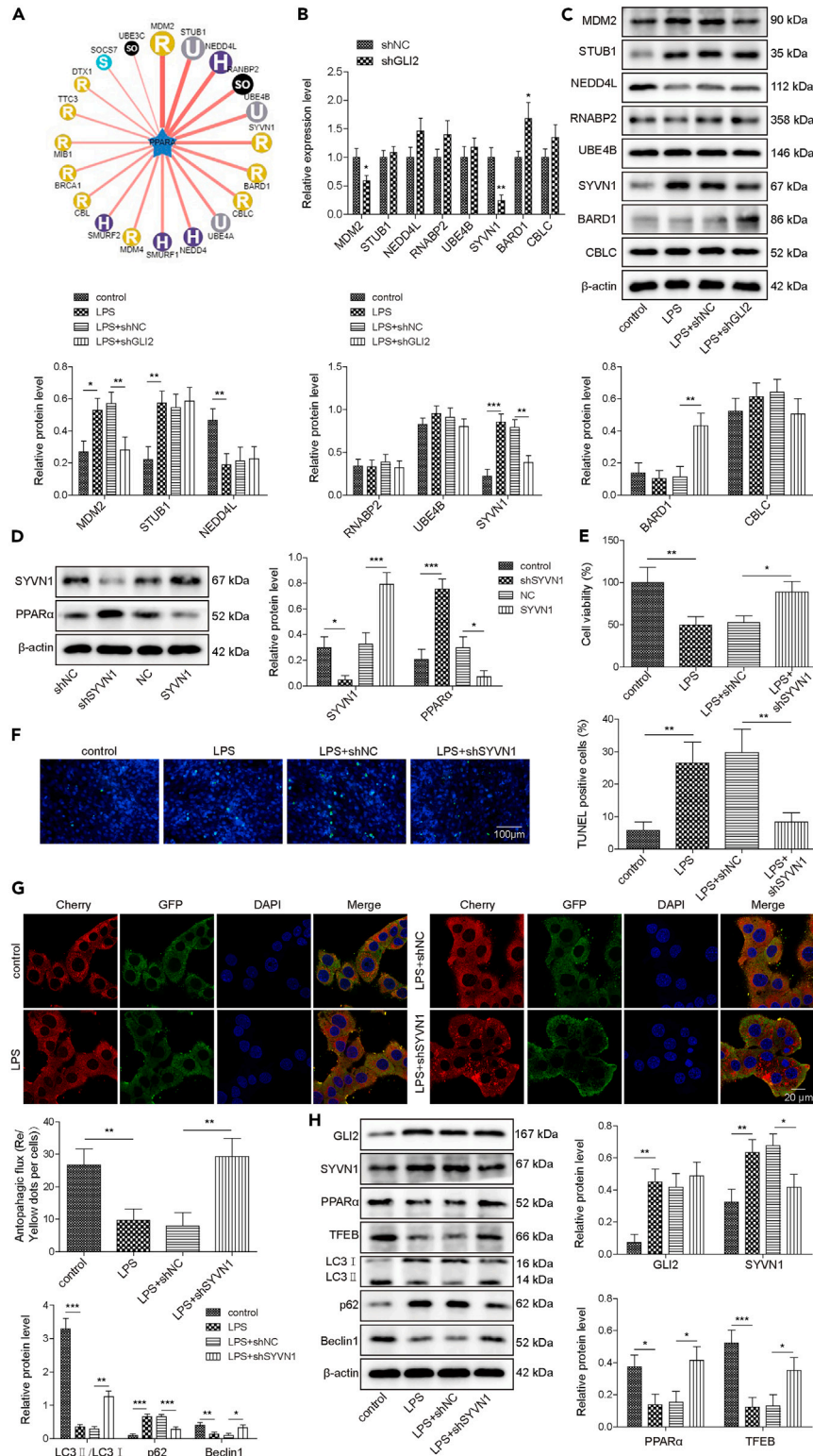


Figure 3. Knockdown of SYVN1 increased PPAR α expression, promoted autophagy, and alleviated LPS-induced septic liver injury *in vitro*

(A) UbiBrowser database predicted eight potential E3 ligases of PPAR α in the confidence mode.

(B) The mRNA levels of these E3 ligases in primary hepatocytes transfected with shGLI2 were detected by RT-qPCR. Hepatocytes were treated with LPS (5 μ g/mL), LPS + shNC, and LPS + shGLI2, then (C) protein levels of these E3 ligases in primary hepatocytes were detected by Western blotting. β -actin served as loading controls.

Figure 3. Continued

(D) Western blotting analysis of SYVN1 and PPAR α expression in hepatocytes transfected with shSYVN1 or SYVN1. β -actin served as loading controls. Hepatocytes were treated with LPS (5 μ g/mL), LPS + shNC, and LPS + shSYVN1, then the viability and mortality of treated hepatocytes were assessed by MTT (E) and TUNEL staining (F), respectively. Scale bar, 100 μ m.

(G) Representative images of immunofluorescence staining of LC3 in treated hepatocytes. Scale bar = 20 μ m.

(H) Western blotting analysis of GLI2, SYVN1, PPAR α and autophagy-related proteins expression in treated hepatocytes. β -actin served as loading controls. Mean \pm SD, $n = 3$, * $p < 0.05$, ** $p < 0.01$, *** $p < 0.001$. Statistical analysis was carried out by a Student's t test or a one-way ANOVA.

the viability and repressed the mortality (Figures 2C and 2D). The autophagosomes were labeled with LC3 punctas. The number of LC3 punctas decreased in cells treated with LPS, while GLI2 silencing partly blocked this autophagic activity decline (Figure 2E). Furthermore, GLI2 knockdown upregulated PPAR α , TFEB, LC3-II/I, and Beclin-1 in LPS-induced cells, while decreasing p62 levels (Figure 2F). Taken together, knockdown of GLI2 enhanced the autophagic activity of hepatocytes and alleviated their injury.

Knockdown of SYVN1 increased PPAR α expression, promoted autophagy, and alleviated LPS-induced septic liver injury in vitro

Considering the low expression of PPAR α , we investigated the effect of PPAR α in LPS-induced hepatocytes. As indicated in Figures S2A and S2B, PPAR α expression were increased in both hepatocytes and those induced by LPS after transfecting with PPAR α plasmid. Overexpression of PPAR α facilitated the viability of LPS-induced hepatocytes and inhibited cell mortality (Figures S2C and S2D). Moreover, PPAR α overexpression increased the number of LC3 puncta in LPS-induced hepatocytes (Figure S2E). AMPK and mTOR have been suggested to promote and inhibit autophagy, respectively.²² We observed that PPAR α overexpression increased the expression of TFEB, LC3-II/I, and Beclin-1 in LPS-induced cells, while repressing p62 expression. Besides, PPAR α overexpression has no effect on the level of p -AMPK α and p -mTOR (Figure S2F). Thus, PPAR α overexpression promoted autophagy under LPS-induced conditions.

The differential expression of SYVN1 was observed in CLP-induced septic mice.²¹ Intriguingly, the UbiBrowser database predicted several potential E3 ligases of PPAR α in the confidence mode, SYVN1 being one of them (Figure 3A). We then selected the eight E3 ligases with the highest reliability, and upon silencing GLI2, found that its suppression led to reduced murine double minute 2 (MDM2) and SYVN1 expressions, with SYVN1 being more pronounced (Figure 3B). While LPS induction elevated MDM2, STIP1 homology and U-Box containing protein 1 (STUB1), and SYVN1 levels, silencing GLI2 decreased both MDM2 and SYVN1 expression, especially SYVN1 expression (Figure 3C). Consequently, SYVN1 was chosen for subsequent study. The plasmids shSYVN1 or SYVN1 were transfected into primary hepatocytes to modulate SYVN1 levels. As indicated in Figure 3D, SYVN1 was downregulated after transfecting with shSYVN1, and its knockdown upregulated PPAR α ; conversely, PPAR α expression decreased following SYVN1 overexpression. Moreover, knockdown of SYVN1 increased the viability of hepatocytes induced by LPS (Figure 3E), while repressing cell mortality (Figure 3F). Knockdown of SYVN1 increased the number of LC3 punctas, suggesting the promoting effect on cell autophagy (Figure 3G). In addition, SYVN1 knockdown promoted the expression of PPAR α , TFEB, LC3-II/I, and Beclin-1 in LPS-induced cells, while inhibiting p62 expression (Figure 3H). Therefore, SYVN1 inhibited cell autophagy by downregulating PPAR α in LPS-induced primary hepatocytes.

GLI2 increased SYVN1 levels by binding with its promoter, thereby promoting ubiquitinated degradation of PPAR α

As shown in Figures 3B and 3C, knockdown of GLI2 reduced SYVN1 levels. We thus began to explore the regulatory relationship between GLI2 and SYVN1. Firstly, the co-immunoprecipitation (Co-IP) experiment in 293T cells revealed that exogenous and endogenous SYVN1 interacted with PPAR α (Figures 4A and 4B). Subsequently, 293T cells were treated with MG132 or CQ, followed by the assessment of PPAR α expression levels. We observed a significant increase in PPAR α expression following MG132 treatment. Interestingly, there is no change in PPAR α expression after treating with CQ (Figure 4C). These findings suggested that PPAR α primarily degraded through the proteasomal pathway. Moreover, the degradation of PPAR α was inhibited with the addition of protein synthesis inhibitor CHX in cells treated with MG132 (Figure 4D). CHX chase assay was also performed in hepatocytes transfected with shNC or shSYVN1, and then we observed that the degradation of PPAR α was reduced after knocking down SYVN1 (Figure 4E). 293T cells were then transfected with Myc-PPAR α , SFB-SYVN1, and HA-ubiquitin. As shown in Figure 4F, SYVN1 promoted the ubiquitination degradation of PPAR α , indicating that the enzymatic activity of SYVN1 is essential for the ubiquitination of PPAR α . Given that K48 and K63 are the most well-characterized branched ubiquitin chains, we further investigated the contribution of these two polyubiquitin linkages in the SYVN1-catalyzed ubiquitination of PPAR α using ubiquitin mutants containing lysine-to-arginine substitutions of all lysine residues except lysine 48 (ubiquitin K48) or lysine 63 (ubiquitin K63). The results showed that under the catalysis of SYVN1, the conjugation efficiency of WT ubiquitin or ubiquitin containing only K48 to PPAR α was high, while the conjugation efficiency of ubiquitin containing only K63 to PPAR α was low (Figure S3A). Consistently, mutation of lysine 48 (K48R), but not lysine 63 (K63R), of ubiquitin abolished its conjugation to PPAR α by SYVN1 (Figure S3B). These results indicated that SYVN1 predominantly conjugates K48-linked polyubiquitin chains to PPAR α . In addition, we also found that the degradation of PPAR α could result in a significant reduction of TFEB (Figures S3A and S3B), suggesting PPAR α caused a reduction of autophagic activity. Afterward, three binding sites between GLI2 and SYVN1 were predicted (Figure 4G). Chromatin immunoprecipitation (ChIP) analyzed the enrichment of GLI2 at three binding sites and then confirmed the GLI2 enrichment at BS1 site (–1153/-1147, GCCAATC) (Figure 4H). The dual-luciferase reporter assay revealed that shGLI2 transfection inhibited SYVN1 WT luciferase activities, but did not change SYVN1 MUT luciferase activities, suggesting that GLI2 knockdown decreased the binding between GLI2 and SYVN1 promoter region.

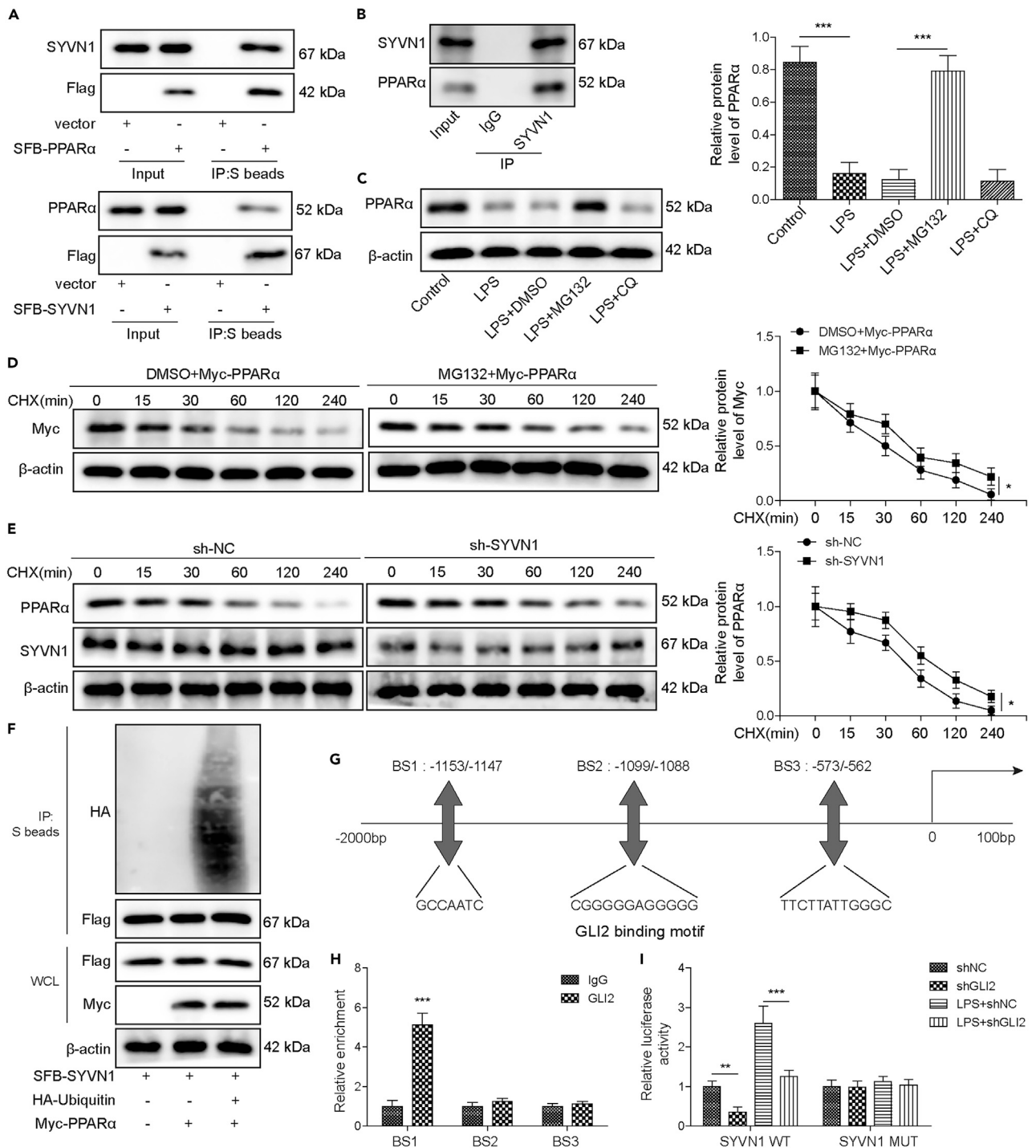


Figure 4. GLI2 increased SYVN1 levels by binding to its promoter, thereby promoting ubiquitinated degradation of PPAR α

(A and B) Co-IP analyzed the exogenous and endogenous interaction between SYVN1 and PPAR α in 293T cells and primary hepatocytes. (C) 293T cells were treated with the proteasome inhibitor MG132 (10 μ M) or autophagy-lysosomal inhibitor Chloroquine (CQ, 50 μ M), cell lysates were subjected to Western blotting to measure PPAR α expression. (D) The protein synthesis inhibitor CHX (30 μ g/mL) chase experiment was conducted in 293T cells treated with MG132 and PPAR α protein levels were assessed by Western blotting. (E) PPAR α protein expression in hepatocytes silenced SYVN1 was determined by using CHX at indicated time points. (F) 293T cells were transfected with SFB-SYVN1 and HA-ubiquitin and then subjected to Co-IP assay for determining the ubiquitinated degradation of PPAR α .

Figure 4. Continued

(G) The binding sites between GLI2 and SYVN1 were predicted.

(H) ChIP analyzed the enrichment of GLI2 at three genomic sites. IgG used as a control.

(I) Luciferase activity of LPS-induced hepatocytes silenced GLI2 was determined after transfecting with SYVN1-Wt and SYVN1-Mut. Mean \pm SD, $n = 3$, * $p < 0.05$, ** $p < 0.01$, *** $p < 0.001$. Statistical analysis was carried out by a Student's t test or a one-way ANOVA.

However, the binding of them was enhanced in cells treated with LPS (Figure 4I). In conclusion, GLI2 promoted the ubiquitinated degradation of PPAR α by targeted upregulation of SYVN1.

Knockdown of IGF2BP3 promoted PPAR α -mediated autophagy and alleviated LPS-induced septic liver injury by downregulating GLI2

A previous study indicated a link between m6A RNA methylation and the heterogeneity of sepsis [20]. Herein, several m6A reader proteins, including IGF2BP2, IGF2BP3, HNRNPA2B1, HNRNPD, HNRNPK, HNRNPM, and HNRNPA1, that might interact with GLI2 were predicted by StarBase (<https://starbase.sysu.edu.cn/index.php>). We then analyzed GLI2 levels in primary hepatocytes after silencing these proteins and found that only silencing IGF2BP3 led to a decrease in GLI2 mRNA levels (Figure 5A). Further examination proved that IGF2BP3 knockdown also reduced the protein levels of GLI2 (Figure 5B). Next, the m6A modification sites in GLI2 transcripts were observed by SRAMP (<http://www.cuilab.cn/sramp>) (Figure 5C), and the binding motif of IGF2BP3 on GLI2 m6A site was obtained by RMBase (<http://rna.sysu.edu.cn/rmbase/>) as GGACU, which is located at the 3'-UTR. Besides, we found that IGF2BP3 specifically bound to the GLI2 full-length transcripts in primary hepatocytes (Figure 5D). This binding relationship was further supported by RIP assay (Figure 5E). Furthermore, IGF2BP3 bound to the 3'-UTR of GLI2, and their interaction was clearly impaired after depleting m6A motif (Figure 5F). To determine the stability of GLI2 mRNA, actinomycin D (act-D) was added into hepatocytes silenced IGF2BP3. We noted a slower decay rate of GLI2 mRNA in treated cells (Figure 5G). Next, we analyzed the function of IGF2BP3 knockdown on primary hepatocytes treated with LPS. As indicated in Figures 5H and 5I, knockdown of IGF2BP3 facilitated cell viability, while decreasing cell mortality. As expected, knockdown of IGF2BP3 not only increased the number of LC3 punctas reduced by LPS (Figure 5J), but also promoted the expression of PPAR α , TFEB, LC3-II/I, and Beclin-1 in LPS-induced cells, while inhibiting GLI2, SYVN1, and p62 expression (Figure 5K), suggesting that IGF2BP3 knockdown blocked the autophagic activity decline induced by LPS. Taken together, IGF2BP3 recognized and bind to the m6A-modified transcript of GLI2 to regulate its expression, thereby repressing PPAR α -mediated autophagy *in vitro*.

IGF2BP3 promoted SYVN1-mediated ubiquitinated degradation of PPAR α by regulating GLI2, thereby facilitating LPS-induced septic liver injury

To explore the regulatory function of IGF2BP3/SYVN1 axis on primary hepatocytes, rescue assays were performed in cells treated with LPS. Overexpression of SYVN1 blocked the promoting effect of IGF2BP3 knockdown on LPS-treated cell viability and the inhibiting effect on cell mortality (Figures 6A and 6B). In addition, the increased LC3 autophagic activity resulting from IGF2BP3 silencing was hindered by SYVN1 overexpression (Figure 6C). The upregulation of PPAR α , TFEB, LC3-II/I, and Beclin-1 and downregulation of p62 caused by IGF2BP3 knockdown in LPS-induced cells were abolished after overexpressing SYVN1 (Figure 6D). These findings verified a regulatory mechanism of the IGF2BP3/GLI2/SYVN1/PPAR α axis in LPS-induced hepatocyte injury.

IGF2BP3 affected septic liver injury in mice through promoting SYVN1-mediated ubiquitinated degradation of PPAR α

Building upon the mechanism we concluded previously, we began exploring biological function of IGF2BP3/GLI2/SYVN1/PPAR α axis *in vivo*. Mice either underwent CLP surgery or were pre-injected with shNC, shIGF2BP3, or shSYVN1 by intraperitoneal injection 48 h before CLP procedure. Silencing IGF2BP3 or SYVN1 ameliorated the decreased survival rate seen in mice following CLP (Figure 7A). The liver damage triggered by CLP was mitigated when mice were injected with shIGF2BP3 or shSYVN1 (Figure 7B). Moreover, knockdown of IGF2BP3 or SYVN1 suppressing ALT and AST expression in the serum (Figure 7C), while increasing the expression of PPAR α and LC3B in liver tissues of mice underwent CLP (Figure 7D). Besides, the upregulation of IGF2BP3 and GLI2 in liver tissues of mice underwent CLP was inhibited by silencing IGF2BP3 (Figure 7E); the decrease of PPAR α , TFEB, LC3-II/I, and Beclin-1 levels and increase of SYVN1 and p62 levels induced by CLP were also reversed after injecting with shIGF2BP3 or shSYVN1 (Figure 7E). Notably, GLI2 knockdown was also observed to improve the survival and the liver injury of mice underwent CLP (Figures S4A and S4B), reduce ALT and AST expression in the serum (Figure S4C), decrease GLI2, SYVN1, and p62 expression and increase PPAR α , TFEB, Beclin-1 and LC3-II/I levels (Figures S4D and S4E). Therefore, IGF2BP3/GLI2/SYVN1/PPAR α axis reduced survival and aggravated liver injury in septic mice by inhibiting autophagy.

DISCUSSION

At the cellular and molecular dimensions, several pathophysiological processes, such as immune dysfunction, mitochondrial damage, and autophagy, contribute to the onset of sepsis, leading to multi-organ damage.^{23,24} Notably, liver injury emerges as an independent and important risk factor, influencing prognosis for sepsis patients.^{3,25} Earlier studies highlighted the potential protective role of autophagy in sepsis by removing pathogens, neutralizing microbial toxins, regulating cytokine release, and promoting antigen expression.^{26–28} For instance, by genetically ablating the autophagy protein ATG16L1 gene, it was found that mice with autophagy deficiency were more vulnerable to LPS

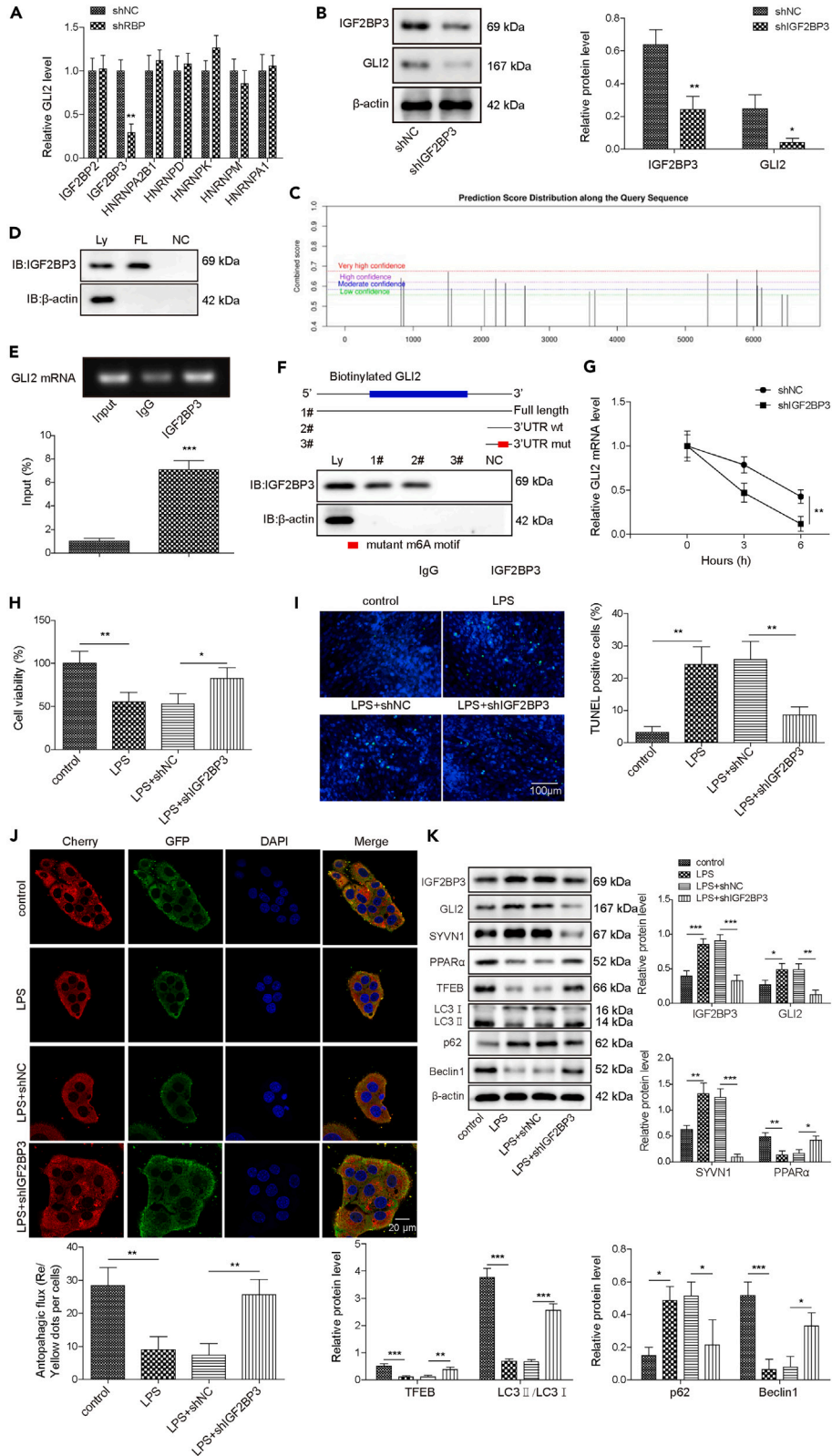


Figure 5. Knockdown of IGF2BP3 promoted PPAR α -mediated autophagy and alleviated LPS-induced septic liver injury by downregulating GLI2 and SYVN1

The potential m6A “reader” proteins that bind to GLI2 mRNA were predicted by StarBase.

(A) The expression of GLI2 in primary hepatocytes was assessed by RT-qPCR after silencing these potential genes.

(B) The protein levels of IGF2BP3 and GLI2 were detected by Western blotting in hepatocytes transfected with shIGF2BP3. β -actin served as loading controls.

(C) The potential m6A modification sites on GLI2 mRNA were predicted by SRAMP (<http://www.cuilab.cn/sramp>).

(D) Immunoblotting of IGF2BP3 after RNA pull-down assay with cell lysate (Ly.), full-length biotinylated-GLI2 (FL), and beads only (NC) in cells.

(E) Agarose electrophoresis and RT-qPCR analysis of RIP assay in cells determined the binding between IGF2BP3 protein and GLI2 mRNA.

(F) Immunoblotting of IGF2BP3 with cell lysate (Ly.), full-length biotinylated-GLI2 (#1), the GLI2 3'-UTR region with or without m6A motif mutation (#2, #3), and beads only (NC) in cells.

(G) Primary hepatocytes transfected with shIGF2BP3 were treated with actinomycin D for indicated times, and GLI2 levels were measured by RT-qPCR. Hepatocytes were treated with LPS (5 μ g/mL), LPS+shNC, and LPS+shIGF2BP3, then the viability and mortality of treated hepatocytes were assessed by MTT (H) and TUNEL staining (I), respectively. Scale bar, 100 μ m.

(J) Representative images of immunofluorescence staining of LC3 in treated hepatocytes. Scale bar, 20 μ m.

(K) Western blotting analysis of IGF2BP3, GLI2, SYVN1, PPAR α and autophagy-related proteins expression in treated hepatocytes. β -actin served as loading controls. Mean \pm SD, $n = 3$, * $p < 0.05$, ** $p < 0.01$, *** $p < 0.001$. Statistical analysis was carried out by a Student's t test or a one-way ANOVA.

challenge.²⁹ The autophagy enhancer CBZ has been proposed to alleviate liver injury in mice with CLP induced-sepsis.⁴ In this study, IGF2BP3 increased GLI2 levels by recognizing and binding to the m6A-modified transcript of GLI2, overexpressed GLI2 subsequently promoted the expression of SYVN1, thereby exacerbating liver injury in sepsis through repressing PPAR α -mediated autophagy.

A previous study has demonstrated the downregulation of PPAR α in septic mice, and its upregulation proved beneficial for mortality rates in CLP-induced peritonitis sepsis mouse models.⁸ Herein, we observed not only the low expression of PPAR α in septic mouse and cell models but also the heightened presence of GLI2. As a primary effector of the Hh pathway, GLI2 has been recognized as a key transcription factor in regulating liver fibrosis. Yan et al. revealed that the deletion of GLI2 in hepatic stellate cells (HSCs) ameliorated CCl₄-induced liver fibrosis and HSCs activation.³⁰ Our findings indicated that GLI2 knockdown improved LPS-induced septic liver injury in primary hepatocytes. Intriguingly, GLI2 knockdown promoted cell autophagy and increased PPAR α levels. Indeed, PPAR α was demonstrated to regulate the transcription of autophagic gene networks in several diseases.³¹ For example, PPAR α agonists gemfibrozil improved memory deficits and anxiety symptoms of Alzheimer disease mice by regulating autophagy in the nervous system.⁵ Importantly, PPAR α has been suggested to activate hepatic autophagy. The suppression of liver autophagy was accompanied by repression of multiple downstream target genes, such as PPAR α and LXR α .³² We therefore concluded that knockdown of GLI2 potentially ameliorated hepatocyte injury by promoting PPAR α -mediated autophagy.

Increasing evidence points to the central role of ubiquitin proteasome system in modulating PPAR α activity.³³ Gopinathan et al. suggested a regulatory relationship between PPAR α and MDM2 (a ubiquitin ligase), revealing that increased MDM2 expression promoted PPAR α ubiquitination.³⁴ Here, several potential E3 ligases of PPAR α were predicted, among which SYVN1 expression was most clearly regulated by GLI2. During sepsis, SYVN1 expression might be triggered by inflammatory cytokines, leading to the degradation of NRF2 and PGC-1 β in the skeletal muscle tissue.²¹ Furthermore, SYVN1 performs different functions in different cells by targeting many substrates, such as a pro-apoptotic factor (IRE1)³⁵ and mitochondrial antiviral signaling (MAVS).³⁶ Concurrently, the involvement of ubiquitin as a targeting signal for selective autophagy is rapidly emerging.^{37–39} Herein, GLI2 activated SYVN1 by binding to its promoter, thereby promoting ubiquitinated degradation of PPAR α . Intriguingly, PPAR α has been indicated to transcriptionally activate TFEB, which enhance lysosome biogenesis and autophagy.⁷ Therefore, GLI2 knockdown promoted TFEB-mediated autophagy through increasing its expression by PPAR α /SYVN1 axis. Our research introduced a novel pathogenesis of septic liver injury rooted in PPAR α degradation mediated by SYVN1.

The m6A mechanism is implicated in the regulation of RNA splicing, RNA degradation and translation through its writer, eraser, and reader proteins.^{14,40–42} m6A RNA methylation was accountable for the heterogeneity of sepsis.¹⁸ Interestingly, IGF2BP3, a recognized m6A reader elevated during sepsis,¹⁹ was found to bind to the m6A site of GLI2 on the 3'-UTR and promote GLI2 expression by enhancing its mRNA stability in this study. As previously demonstrated, m6A modification of mRNA plays vital functions in sepsis, with m6A-cis-expression quantitative trait loci (eQTL) playing the most pronounced role in individual variants of sepsis progression.⁴³ Our study indicated that IGF2BP3 played a major role in GLI2 mRNA stability via m6A modification in LPS-treated primary hepatocytes and CLP-induced mice. Importantly, IGF2BP3 silencing enhanced PPAR α -mediated autophagic flux and improved liver injury of septic cells and mice to some extent.

Taken together, our findings suggested that IGF2BP3 interacted with GLI2 mRNA and stabilized the expression of m6A-modified RNA, the upregulation of GLI2 transcriptionally promoted SYVN1 levels and subsequently enhanced the degradation of PPAR α , ultimately exacerbating septic liver injury both *in vitro* and *in vivo* through repressing PPAR α -mediated autophagy. These results highlighted the IGF2BP3/GLI2/SYVN1/PPAR α axis as a potential therapeutic target for conquering sepsis.

STAR★METHODS

Detailed methods are provided in the online version of this paper and include the following:

● KEY RESOURCES TABLE

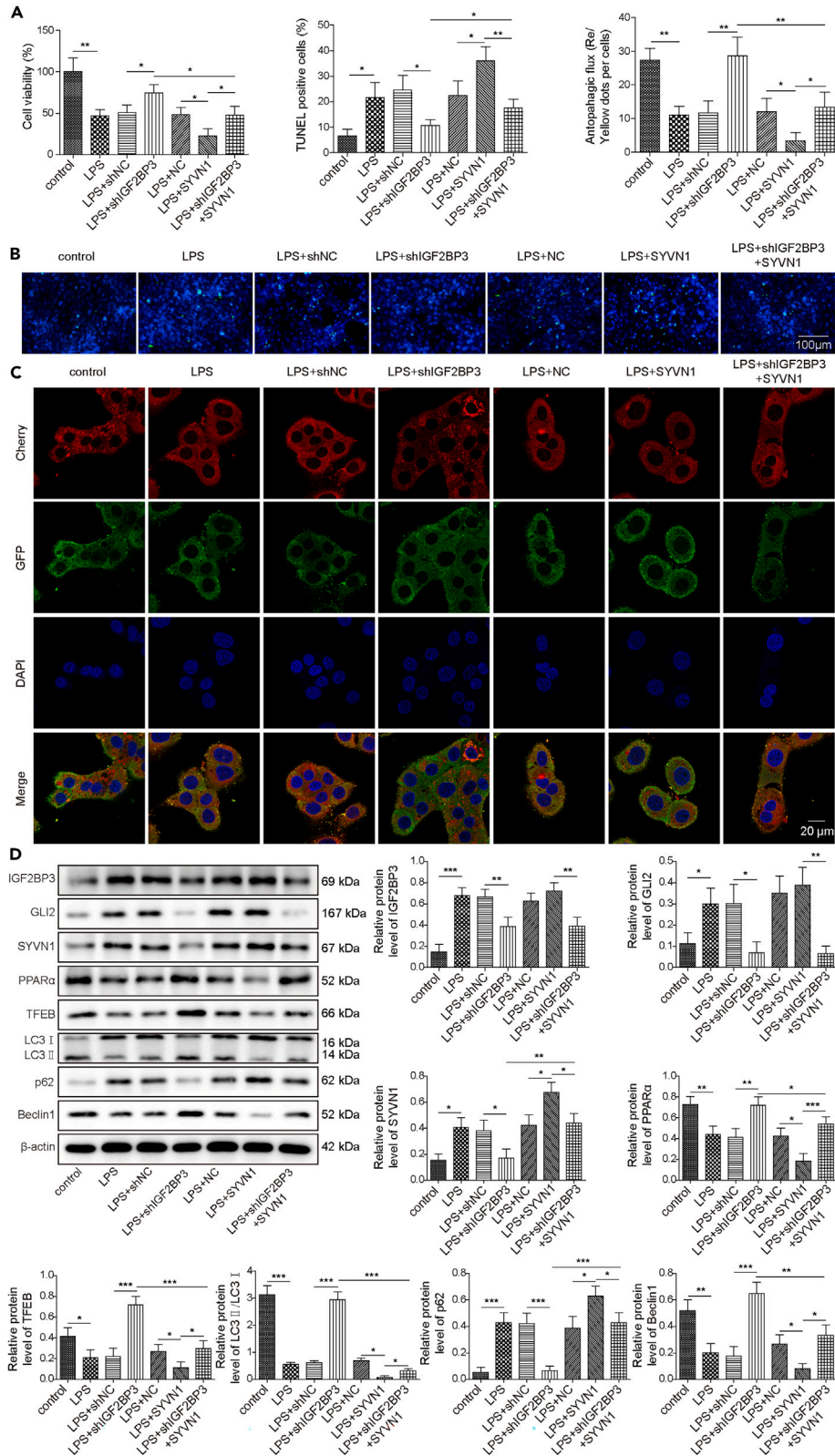


Figure 6. IGF2BP3 promoted SYVN1-mediated ubiquitinated degradation of PPAR α by regulating GLI2, thereby controlling LPS-induced septic liver injury

Hepatocytes were treated with LPS (5 μ g/mL), LPS+shNC, LPS+shIGF2BP3, LPS+NC, LPS+SYVN1, LPS+shIGF2BP3+SYVN1.

(A and B) The viability and mortality of treated hepatocytes were assessed by MTT, and TUNEL staining, respectively. Scale bar, 100 μ m.

(C) Representative images of immunofluorescence staining of LC3 in treated hepatocytes. Scale bar, 20 μ m.

(D) Western blotting analysis of IGF2BP3, GLI2, SYVN1, PPAR α , and autophagy-related proteins expression in treated hepatocytes. β -actin served as loading controls. Mean \pm SD, $n = 3$, * $p < 0.05$, ** $p < 0.01$, *** $p < 0.001$. Statistical analysis was carried out by a one-way ANOVA.

● RESOURCE AVAILABILITY

- Lead contact
- Materials availability
- Data and code availability

● EXPERIMENTAL MODEL AND STUDY PARTICIPANT DETAILS**● METHOD DETAILS**

- *In vivo* mouse model
- Cell culture and treatment
- Cell transfection
- 3-(4,5-Dimethylthiazol-2-yl)-2,5-diphenyltetrazolium bromide (MTT) assay
- Flow cytometric analysis
- TUNEL assay
- Immunofluorescence
- Proteasome and autophagy-lysosomal inhibitor assay
- Chromatin immunoprecipitation assay (ChIP)
- Dual-luciferase reporter assay
- RNA pull-down
- RNA immunoprecipitation (RIP)
- Co-immunoprecipitation (Co-IP)
- Measurement of alanine transaminase (ALT) and aspartate transaminase (AST)
- Histopathological examination
- Immunohistochemistry (IHC)
- Quantitative real-time PCR (RT-qPCR)
- Western blot analysis

● QUANTIFICATION AND STATISTICAL ANALYSIS**SUPPLEMENTAL INFORMATION**

Supplemental information can be found online at <https://doi.org/10.1016/j.isci.2024.109870>.

ACKNOWLEDGMENTS

This work was supported by Natural Science Foundation of Hunan Province, China (grant no. 2023JJ30830, 2021JJ40920), the Project of Hunan Provincial Health Commission (20201585) and the Changsha Municipal Natural Science Foundation (kq2007049).

AUTHOR CONTRIBUTIONS

Guarantor of integrity of the entire study: C.S. and H.L.; study concepts: C.S. and H.L.; study design: C.S. and H.L.; definition of intellectual content: C.S. and R.Z.; literature research: M.G.; clinical studies: C.S. and H.H.; experimental studies: J.Q.; data acquisition: Y.T.; data analysis: C.S. and X.C.; statistical analysis: C.S.; manuscript preparation: H.L.

DECLARATION OF INTERESTS

The authors declare that no competing financial interest exists.

Received: July 29, 2023

Revised: December 14, 2023

Accepted: April 29, 2024

Published: May 3, 2024

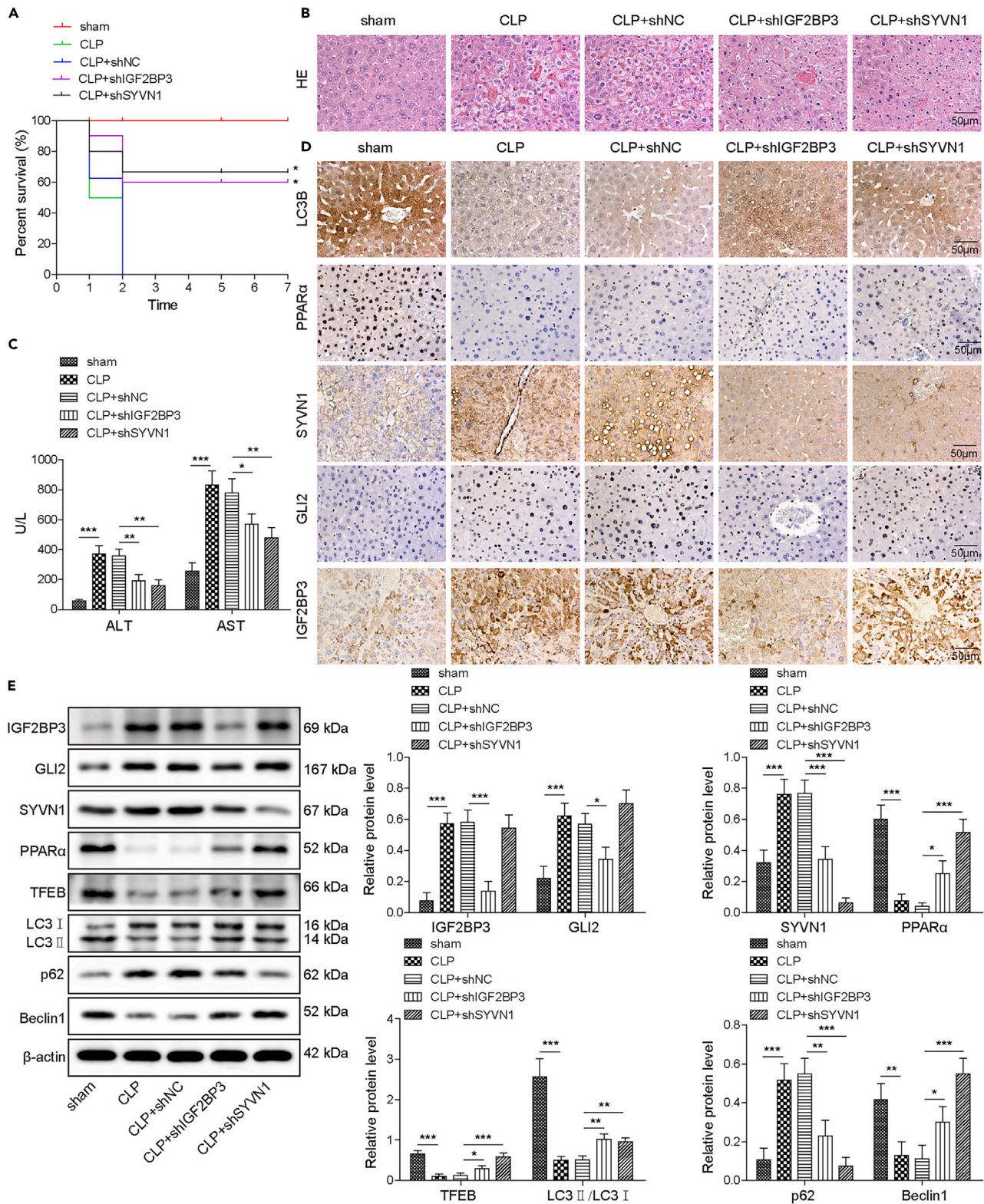


Figure 7. Continued

(A) Kaplan-Meier survival curve of mice in each group.

(B) Pathological changes in liver tissues of each group mice were measured by HE staining. Scale bar, 50 μ m.

(C) The activity of ALT and AST in serum was evaluated by respective kits.

(D) The expression of IGF2BP3, GLI2, SYVN1, and LC3B in liver tissues was assessed by IHC. Scale bar, 50 μ m.

(E) The expression of IGF2BP3, GLI2, SYVN1, PPAR α , and autophagy-related proteins in liver tissues was measured by Western blotting. Blots for β -actin served as loading controls. Mean \pm SD, * p < 0.05, ** p < 0.01, *** p < 0.001. Statistical analysis was carried out by a one-way ANOVA.

REFERENCES

- Blanco, J., Muriel-Bombín, A., Sagredo, V., Taboada, F., Gandía, F., Tamayo, L., Collado, J., García-Labattut, A., Carriedo, D., Valledor, M., et al. (2008). Incidence, organ dysfunction and mortality in severe sepsis: a Spanish multicentre study. *Crit. Care* 12, R158. <https://doi.org/10.1186/cc7157>.
- Kramer, L., Jordan, B., Druml, W., Bauer, P., and Metnitz, P.G.H.; Austrian Epidemiologic Study on Intensive Care ASDI Study Group (2007). Incidence and prognosis of early hepatic dysfunction in critically ill patients—a prospective multicenter study. *Crit. Care Med.* 35, 1099–1104. <https://doi.org/10.1097/01.CCM.0000259462.97164.A0>.
- Yan, J., Li, S., and Li, S. (2014). The role of the liver in sepsis. *Int. Rev. Immunol.* 33, 498–510. <https://doi.org/10.3109/08830185.2014.889129>.
- Lin, C.W., Lo, S., Perng, D.S., Wu, D.B.C., Lee, P.H., Chang, Y.F., Kuo, P.L., Yu, M.L., Yuan, S.S.F., and Hsieh, Y.C. (2014). Complete activation of autophagic process attenuates liver injury and improves survival in septic mice. *Shock* 41, 241–249. <https://doi.org/10.1097/SHK.0000000000000111>.
- Luo, R., Su, L.Y., Li, G., Yang, J., Liu, Q., Yang, L.X., Zhang, D.F., Zhou, H., Xu, M., Fan, Y., et al. (2020). Activation of PPARA-mediated autophagy reduces Alzheimer disease-like pathology and cognitive decline in a murine model. *Autophagy* 16, 52–69. <https://doi.org/10.1080/15548627.2019.1596488>.
- You, M., Gao, J., Jin, J., and Hou, Y. (2018). PPARalpha Enhances Cancer Cell Chemotherapy Sensitivity by Autophagy Induction. *J. Oncol.* 2018, 6458537. <https://doi.org/10.1155/2018/6458537>.
- Tao, H., Yancey, P.G., Blakemore, J.L., Zhang, Y., Ding, L., Jerome, W.G., Brown, J.D., Vickers, K.C., and Linton, M.F. (2021). Macrophage SR-BI modulates autophagy via VPS34 complex and PPARalpha transcription of Tfcb in atherosclerosis. *J. Clin. Invest.* 131, e94229. <https://doi.org/10.1172/JCI94229>.
- Van Wyngene, L., Vanderhaeghen, T., Timmermans, S., Vandewalle, J., Van Looveren, K., Souffriau, J., Wallaëys, C., Eggermont, M., Ernst, S., Van Hamme, E., et al. (2020). Hepatic PPARalpha function and lipid metabolic pathways are dysregulated in polymicrobial sepsis. *EMBO Mol. Med.* 12, e11319. <https://doi.org/10.15252/emmm.201911319>.
- Omenetti, A., Choi, S., Michelotti, G., and Diehl, A.M. (2011). Hedgehog signaling in the liver. *J. Hepatol.* 54, 366–373. <https://doi.org/10.1016/j.jhep.2010.10.003>.
- Cai, Y., Zheng, H., Gong, W., Che, Y., and Jiang, B. (2011). The role of hedgehog signaling pathway in liver regeneration. *Hepato-Gastroenterology* 58, 2071–2076. <https://doi.org/10.5754/hge11155>.
- Michelotti, G.A., Xie, G., Swiderska, M., Choi, S.S., Karaca, G., Krüger, L., Premont, R., Yang, L., Syn, W.K., Metzger, D., and Diehl, A.M. (2013). Smoothed is a master regulator of adult liver repair. *J. Clin. Invest.* 123, 2380–2394. <https://doi.org/10.1172/JCI66904>.
- Peterson, K.A., Nishi, Y., Ma, W., Vedenko, A., Shokri, L., Zhang, X., McFarlane, M., Baizabal, J.M., Junker, J.P., van Oudenaarden, A., et al. (2012). Neural-specific Sox2 input and differential Gli-binding affinity provide context and positional information in Shh-directed neural patterning. *Genes Dev.* 26, 2802–2816. <https://doi.org/10.1101/gad.207142.112>.
- Jiayuan, S., Junyan, Y., Xiangzhen, W., Zuping, L., Jian, N., Baowei, H., and Lifang, J. (2020). Gant61 ameliorates CCl(4)-induced liver fibrosis by inhibition of Hedgehog signaling activity. *Toxicol. Appl. Pharmacol.* 387, 114853. <https://doi.org/10.1016/j.taap.2019.114853>.
- Huang, H., Weng, H., Sun, W., Qin, X., Shi, H., Wu, H., Zhao, B.S., Mesquita, A., Liu, C., Yuan, C.L., et al. (2018). Recognition of RNA N(6)-methyladenosine by IGF2BP proteins enhances mRNA stability and translation. *Nat. Cell Biol.* 20, 285–295. <https://doi.org/10.1038/s41556-018-0045-z>.
- Gao, Y., Luo, T., Ouyang, X., Zhu, C., Zhu, J., and Qin, X. (2020). IGF2BP3 and miR191-5p synergistically increase HCC cell invasiveness by altering ZO-1 expression. *Oncol. Lett.* 20, 1423–1431. <https://doi.org/10.3892/ol.2020.11693>.
- Roundtree, I.A., Evans, M.E., Pan, T., and He, C. (2017). Dynamic RNA Modifications in Gene Expression Regulation. *Cell* 169, 1187–1200. <https://doi.org/10.1016/j.cell.2017.05.045>.
- Zaccara, S., Ries, R.J., and Jaffrey, S.R. (2019). Reading, writing and erasing mRNA methylation. *Nat. Rev. Mol. Cell Biol.* 20, 608–624. <https://doi.org/10.1038/s41580-019-0168-5>.
- Zhang, S., Liu, F., Wu, Z., Xie, J., Yang, Y., and Qiu, H. (2020). Contribution of m6A subtype classification on heterogeneity of sepsis. *Ann. Transl. Med.* 8, 306. <https://doi.org/10.21037/atm.2020.03.07>.
- Zhang, S., Guan, X., Liu, W., Zhu, Z., Jin, H., Zhu, Y., Chen, Y., Zhang, M., Xu, C., Tang, X., et al. (2022). YTHDF1 alleviates sepsis by upregulating WWP1 to induce NLRP3 ubiquitination and inhibit caspase-1-dependent pyroptosis. *Cell Death Discov.* 8, 244. <https://doi.org/10.1038/s41420-022-00872-2>.
- Schulz, J., Avci, D., Queisser, M.A., Gutschmidt, A., Dreher, L.S., Fenech, E.J., Volkmar, N., Hayashi, Y., Hoppe, T., and Christianson, J.C. (2017). Conserved cytoplasmic domains promote Hrd1 ubiquitin ligase complex formation for ER-associated degradation (ERAD). *J. Cell Sci.* 130, 3322–3335. <https://doi.org/10.1242/jcs.206847>.
- Ishida, Y., Fujita, H., Aratani, S., Chijiwa, M., Taniguchi, N., Yokota, M., Ogihara, Y., Uoshima, N., Nagashima, F., Uchino, H., and Nakajima, T. (2018). The NRF2-PGC-1beta pathway activates kynurenine aminotransferase 4 via attenuation of an E3 ubiquitin ligase, synoviolin, in a cecal ligation/perforation-induced septic mouse model. *Mol. Med. Rep.* 18, 2467–2475. <https://doi.org/10.3892/mmr.2018.9175>.
- Kim, J., Kundu, M., Viollet, B., and Guan, K.L. (2011). AMPK and mTOR regulate autophagy through direct phosphorylation of Ulk1. *Nat. Cell Biol.* 13, 132–141. <https://doi.org/10.1038/ncb2152>.
- Huang, M., Cai, S., and Su, J. (2019). The Pathogenesis of Sepsis and Potential Therapeutic Targets. *Int. J. Mol. Sci.* 20, 5376. <https://doi.org/10.3390/ijms20215376>.
- Liu, J., Wu, Q., Shi, J., Guo, W., Jiang, X., Zhou, B., and Ren, C. (2020). LILRB4, from the immune system to the disease target. *Am. J. Transl. Res.* 12, 3149–3166.
- Li, J., Lu, Y., and Lin, G. (2022). Blocking cGAS/STING signaling protects against sepsis-associated acute liver injury. *Int. Immunopharmacol.* 113, 109276. <https://doi.org/10.1016/j.intimp.2022.109276>.
- Maurer, K., Reyes-Robles, T., Alonzo, F., 3rd, Durbin, J., Torres, V.J., and Cadwell, K. (2015). Autophagy mediates tolerance to *Staphylococcus aureus* alpha-toxin. *Cell Host Microbe* 17, 429–440. <https://doi.org/10.1016/j.chom.2015.03.001>.
- Nakahira, K., Haspel, J.A., Rathinam, V.A.K., Lee, S.J., Dolinay, T., Lam, H.C., Englert, J.A., Rabinovitch, M., Cernadas, M., Kim, H.P., et al. (2011). Autophagy proteins regulate innate immune responses by inhibiting the release of mitochondrial DNA mediated by the NALP3 inflammasome. *Nat. Immunol.* 12, 222–230. <https://doi.org/10.1038/ni.1980>.
- Ryter, S.W., Mizumura, K., and Choi, A.M.K. (2014). The impact of autophagy on cell death modalities. *Int. J. Cell Biol.* 2014, 502676. <https://doi.org/10.1155/2014/502676>.
- Schafer, S.T., Franken, L., Adamzik, M., Schumak, B., Scherag, A., Engler, A., Schonborn, N., Walden, J., Koch, S., Baba, H.A., et al. (2016). Mitochondrial DNA: An Endogenous Trigger for Immune Paralysis. *Anesthesiology* 124, 923–933. <https://doi.org/10.1097/ALN.0000000000001008>.
- Yan, J., Hu, B., Shi, W., Wang, X., Shen, J., Chen, Y., Huang, H., and Jin, L. (2021). Gli2-regulated activation of hepatic stellate cells and liver fibrosis by TGF-beta signaling. *Am. J. Physiol. Gastrointest. Liver Physiol.* 320, G720–G728. <https://doi.org/10.1152/ajpgi.00310.2020>.
- Gou, Q., Jiang, Y., Zhang, R., Xu, Y., Xu, H., Zhang, W., Shi, J., and Hou, Y. (2020). PPARdelta is a regulator of autophagy by its phosphorylation. *Oncogene* 39, 4844–4853. <https://doi.org/10.1038/s41388-020-1329-x>.
- Byrnes, K., Blessinger, S., Bailey, N.T., Scaife, R., Liu, G., and Khambu, B. (2022). Therapeutic regulation of autophagy in

- hepatic metabolism. *Acta Pharm. Sin. B* 12, 33–49. <https://doi.org/10.1016/j.apsb.2021.07.021>.
33. Blanquart, C., Barbier, O., Fruchart, J.C., Staels, B., and Glineur, C. (2002). Peroxisome proliferator-activated receptor alpha (PPARalpha) turnover by the ubiquitin-proteasome system controls the ligand-induced expression level of its target genes. *J. Biol. Chem.* 277, 37254–37259. <https://doi.org/10.1074/jbc.M110598200>.
 34. Gopinathan, L., Hannon, D.B., Peters, J.M., and Vanden Heuvel, J.P. (2009). Regulation of peroxisome proliferator-activated receptor-alpha by MDM2. *Toxicol. Sci.* 108, 48–58. <https://doi.org/10.1093/toxsci/kfn260>.
 35. Gao, B., Lee, S.M., Chen, A., Zhang, J., Zhang, D.D., Kannan, K., Ortmann, R.A., and Fang, D. (2008). Synoviolin promotes IRE1 ubiquitination and degradation in synovial fibroblasts from mice with collagen-induced arthritis. *EMBO Rep.* 9, 480–485. <https://doi.org/10.1038/embor.2008.37>.
 36. Luo, Z., Liu, L.F., Jiang, Y.N., Tang, L.P., Li, W., Ouyang, S.H., Tu, L.F., Wu, Y.P., Gong, H.B., Yan, C.Y., et al. (2020). Novel insights into stress-induced susceptibility to influenza: corticosterone impacts interferon-beta responses by Mfn2-mediated ubiquitin degradation of MAVS. *Signal Transduct. Target. Ther.* 5, 202. <https://doi.org/10.1038/s41392-020-00238-z>.
 37. Fujita, N., and Yoshimori, T. (2011). Ubiquitination-mediated autophagy against invading bacteria. *Curr. Opin. Cell Biol.* 23, 492–497. <https://doi.org/10.1016/j.ceb.2011.03.003>.
 38. Feng, L., Zhang, J., Zhu, N., Ding, Q., Zhang, X., Yu, J., Qiang, W., Zhang, Z., Ma, Y., Huang, D., et al. (2017). Ubiquitin ligase SYVN1/HRD1 facilitates degradation of the SERPINA1 Z variant/alpha-1-antitrypsin Z variant via SQSTM1/p62-dependent selective autophagy. *Autophagy* 13, 686–702. <https://doi.org/10.1080/15548627.2017.1280207>.
 39. Li, H., Roy, M., Liang, L., Cao, W., Hu, B., Li, Y., Xiao, X., Wang, H., Ye, M., Sun, S., et al. (2022). Deubiquitylase USP12 induces pro-survival autophagy and bortezomib resistance in multiple myeloma by stabilizing HMGB1. *Oncogene* 41, 1298–1308. <https://doi.org/10.1038/s41388-021-02167-9>.
 40. Bartosovic, M., Molares, H.C., Gregorova, P., Hrossova, D., Kudla, G., and Vanacova, S. (2017). N6-methyladenosine demethylase FTO targets pre-mRNAs and regulates alternative splicing and 3'-end processing. *Nucleic Acids Res.* 45, 11356–11370. <https://doi.org/10.1093/nar/gkx778>.
 41. Choe, J., Lin, S., Zhang, W., Liu, Q., Wang, L., Ramirez-Moya, J., Du, P., Kim, W., Tang, S., Sliz, P., et al. (2018). mRNA circularization by METTL3-elf3h enhances translation and promotes oncogenesis. *Nature* 561, 556–560. <https://doi.org/10.1038/s41586-018-0538-8>.
 42. He, L., Li, H., Wu, A., Peng, Y., Shu, G., and Yin, G. (2019). Functions of N6-methyladenosine and its role in cancer. *Mol. Cancer* 18, 176. <https://doi.org/10.1186/s12943-019-1109-9>.
 43. Sun, X., Dai, Y., Tan, G., Liu, Y., and Li, N. (2020). Integration Analysis of m(6)A-SNPs and eQTLs Associated With Sepsis Reveals Platelet Degranulation and Staphylococcus aureus Infection are Mediated by m(6)A mRNA Methylation. *Front. Genet.* 11, 7. <https://doi.org/10.3389/fgene.2020.00007>.

STAR★METHODS

KEY RESOURCES TABLE

REAGENT or RESOURCE	SOURCE	IDENTIFIER
<i>Antibodies</i>		
GLI2	ThermoFisher	Cat# PA1-28838; RRID: AB_2111904
PPAR α	ThermoFisher	Cat# MA5-37652; RRID: AB_2897578
TFEB	Abcam	Cat# ab56330; RRID: AB_945802
LC3-II/I	Abcam	Cat# ab128025; RRID: AB_11143008
p62	Abcam	Cat# ab109012; RRID: AB_2810880
Beclin-1	Abcam	Cat# ab302669; RRID: AB_302669
AMPK α	Abcam	Cat# ab32047; RRID: AB_722764
p-AMPK α	Abcam	Cat# ab133448; RRID: AB_2923300
mTOR	Abcam	Cat#ab32028; RRID: AB_881283
p-mTOR	Abcam	Cat#ab109268; RRID: AB_10888105
MDM2	Abcam	Cat#ab259265; RRID: AB_2920616
STUB1	Abcam	Cat#ab134064; RRID: AB_2751008
NEDD4L	ThermoFisher	Cat#MA5-32294; RRID: AB_2809579
RANBP2	ThermoFisher	Cat#PA1-082; RRID: AB_325806
UBE4B	Abcam	Cat#ab126759; RRID: AB_11144331
SYVN1	ThermoFisher	Cat#13473-1-AP; RRID: AB_2287023
BARD1	Abcam	Cat#ab ab78176; RRID: AB_2061242
CBLC	ThermoFisher	Cat#PA5-87032; RRID: AB_2803786
IGF2BP3	ThermoFisher	Cat#MA5-27481; RRID: AB_2723272
HRP-conjugated secondary antibody	Santa Cruz Biotechnology	Cat# sc2004; RRID: AB_631746
LC3B	Abcam	Cat# ab192890; RRID: AB_2827794
HA	Abcam	Cat# ab9110; RRID: AB_307019
Flag	Cell Signaling Technology	Cat# 2044; RRID: AB_10707327
Myc	Sigma Aldrich	Cat# M4439; RRID: AB_439694
IgG	ThermoFisher	Cat# 14678-1-AP; RRID: AB_1851235
β -actin	Abcam	Cat# ab8226; RRID: AB_306371
<i>Chemicals, peptides, and recombinant proteins</i>		
MG132	Sigma Aldrich	Cat# M7449
CQ	Sigma Aldrich	Cat# C6628
lipopolysaccharide	medchemexpress	Cat# HY-D1056
Lipofectamine 3000 reagent	Invitrogen	Cat# L3000150
MTT	Beyotime	Cat# C0009M
ECL	Beyotime	Cat# P0018S
SYBR Green qPCR	Applied Biosystems	Cat# 4309155
<i>Critical commercial assays</i>		
Annexin V/ PI apoptosis detection kit	Nanjing Jiancheng Biotech	Cat# G003-1-2
Alanine transaminase (ALT) kit	Nanjing Jiancheng Biotech	Cat# C009-3-1
Aspartate transaminase (AST) kit	Nanjing Jiancheng Biotech	Cat# C010-3-1
EdUTP TUNEL cell detection kit	Ribobio	Cat# C11026-2
Magna RIP Kit	Millipore	Cat# 17-701
RNA Pull-down Kit	Pierce	Cat# 20164

(Continued on next page)

Continued

REAGENT or RESOURCE	SOURCE	IDENTIFIER
ChIP Assay Kit	Pierce	Cat# 26159
Deposited data		
StarBase	This paper	Figure 5A; https://starbase.sysu.edu.cn/index.php
hTFtarget	This paper	Figure 4G; http://bioinfo.life.hust.edu.cn/hTFtarget#!/
ubibrowser	This paper	Figure 3A; http://ubibrowser.bio-it.cn/ubibrowser/home/index
SRAMP	This paper	Figure 5C; http://www.cuilab.cn/sramp
RMBase	This paper	Figure 5D; http://ma.sysu.edu.cn/rmbase/
Experimental models: Cell lines		
HEK293T	ATCC	Cat# CRL-3216
Experimental models: Organisms/strains		
male BABL/c mice	Hunan SJA laboratory animal Co., Ltd	N/A
Oligonucleotides		
shRNA targeting sequence: GLI2: 5'- TCGACCTACAACGCATGATTC-3'	This paper	N/A
shRNA targeting sequence: SYVN1: 5'- GCTGGTATTGGCTTTGAGTA-3'	This paper	N/A
shRNA targeting sequence: IGF2BP3: 5'- CGCGGAGAAGTCCACTACTAT-3'	This paper	N/A
shRNA targeting sequence: IGF2BP2: 5'- GCCGCATGATTCTTGAGATTA-3'	This paper	N/A
shRNA targeting sequence: HNRNPA2B1: 5'- CATTCCATTGATGCCAGGGTA-3'	This paper	N/A
shRNA targeting sequence: HNRNPD: 5'- CACAATGTTGGTCTTAGTAAA-3'	This paper	N/A
shRNA targeting sequence: HNRNPK: 5'- CGGATTAACAAAATTCGTCAT-3'	This paper	N/A
shRNA targeting sequence: HNRNPM: 5'- GCCGAATAAATGAAATCCTAA-3'	This paper	N/A
shRNA targeting sequence: HNRNPA1: 5'- GCCACAACGTGAAGTAAGAA-3'	This paper	N/A
BS1(ChIP): GCCAATC	This paper	N/A
BS2(ChIP): CGGGGGAGGGGG	This paper	N/A
BS3(ChIP): TTCTTATTGGGC	This paper	N/A
Primers for MDM2, see Table S2	This paper	N/A
Primers for STUB1, see Table S2	This paper	N/A
Primers for NEDD4L, see Table S2	This paper	N/A
Primers for RANBP2, see Table S2	This paper	N/A
Primers for UBE4B, see Table S2	This paper	N/A
Primers for SYVN1, see Table S2	This paper	N/A

(Continued on next page)

Continued

REAGENT or RESOURCE	SOURCE	IDENTIFIER
Primers for BARD1, see Table S2	This paper	N/A
Primers for CBLC, see Table S2	This paper	N/A
Primers for GLI2, see Table S2	This paper	N/A
Primers for GAPDH, see Table S2	This paper	N/A
Recombinant DNA		
Plasmid: pGL3 vector	YouBio	Cat# VT1554
Plasmid: pcDNA3.1	YouBio	Cat# VT1001
pGLVH1 vector	Genepharma	Cat# C06003
Dual-Luciferase Assay System	Invitrogen	Cat# T1033
Software and algorithms		
ImageJ	Schneider et al. ⁷	https://imagej.nih.gov/ij/
microplate reader	Bio-Rad	N/A
confocal microscopy	Nikon	N/A

RESOURCE AVAILABILITY**Lead contact**

Further information and request for resources and reagents should be directed to and will be fulfilled by the lead contact, Huaizheng Liu (Lhz3385@csu.edu.cn).

Materials availability

This study did not generate new unique reagents.

Data and code availability

- All data reported in this paper will be shared by the [lead contact](#) upon request.
- This paper does not report original code.
- Any additional information required to reanalyze the data reported in this paper is available from the [lead contact](#) upon request.

EXPERIMENTAL MODEL AND STUDY PARTICIPANT DETAILS

The study was approved by the Animal Care and Use Committee of the Third Xiangya Hospital, Central South University (Approval Number: 2022-S373). 35 BABL/c mice (6 weeks, 16-20 g) were obtained from human SJA laboratory animal co., LTD (Hunan, China) and housed under specific pathogen-free conditions. A septic mouse model was established using cecal ligation and puncture (CLP) surgery, with variations in pre-treatment for different groups. Mice in the Sham group underwent laparotomy without cecal ligation and puncture. After a week, mice were euthanized and livers were collected for further analysis.

METHOD DETAILS***In vivo* mouse model**

All mouse-related experiments were approved by the Animal Care and Use Committee of the Third Xiangya Hospital, Central South University Approval for Scientific Research Project Number: 2022-S373. BABL/c mice (6 weeks, 16-20 g) purchased from human SJA laboratory animal co., LTD (Hunan, China) under specific pathogen-free circumstances. Mice were randomly divided into seven groups (n=5): Control, Sham, CLP, CLP + shNC (pre-injected with shNC by intraperitoneal injection 48 h before CLP surgery), CLP+shIGF2BP3 (pre-injected with shIGF2BP3), CLP+shSYVN1 (pre-injected with shSYVN1), and CLP+shGLI2 (pre-injected with shGLI2). CLP surgery was used to establish septic mouse model and performed as follow: we firstly anesthetized mice by intraperitoneally injecting pentobarbital sodium (50 mg/kg). After creating a midline abdominal incision and exposing cecum, ligated below the ileocecal valve and punctured once using a 20-gauge needle. Afterwards, the cecum was placed back and the abdominal wall was then closed. Mouse in sham group was accepted laparotomies and bowel manipulations, but no ligations and perforations were made. After a week, mice were euthanized and livers were collected for further analysis.

Cell culture and treatment

Primary hepatocytes were isolated from 6-8 weeks old mouse livers. Briefly, livers were digested with 0.06% collagenase type IV, followed by removing and chopping up in a dish. After percoll treatment, then, hepatocytes were obtained with 80%–90% viability and

grown in DMEM supplemented with 10% FBS and 0.01 mM dexamethasone. To establish septic cell models, primary hepatocytes were incubated with lipopolysaccharide (LPS) for 8 h at different dosages (0, 1, 5, or 10 $\mu\text{g}/\text{mL}$) and then collected for the indicated experiments.

Cell transfection

Short hairpin RNA (shRNA) targeted GLI2, SYVN1, IGF2BP3, IGF2BP2, HNRNPA2B1, HNRNPD, HNRNPK, HNRNPM, HNRNPA1 (shGLI2, shSYVN1, shIGF2BP3, shIGF2BP2, shHNRNPA2B1, shHNRNPD, shHNRNPK, shHNRNPM, and shHNRNPA1) or scrambled oligonucleotides, purchased from GenePharma (Shanghai, China) were inserted into pGLVH1 vector. The shRNA sequences were provided in [Table S1](#). The full length of SYVN1 or PPAR α coding sequence was amplified and cloned into a pcDNA3.1 (Invitrogen, Carlsbad, CA, USA) vector (SYVN1, PPAR α). Cells were transfected with the above plasmids using Lipofectamine 3000 transfection reagent (Invitrogen) according to manufacturer's instructions. Lenti-Pac HIV Expression Packaging Mix and the lentiviral vectors (shSYVN1, shIGF2BP3, shGLI2) were used to transfect HEK293T cells for 48 hours and then lentiviral particles were harvested from the supernatant. Stable transfected cells were selected by two weeks puromycin treatment (2 $\mu\text{g}/\text{mL}$).

3-(4,5-Dimethylthiazol-2-yl)-2,5-diphenyltetrazolium bromide (MTT) assay

Treated cells seeded on 96-well plate were incubated with MTT solution (0.5 mg/mL) for 4h. After that, the non-soluble crystals were solubilizing by centrifugating and adding 150 μL of DMSO. The absorption was assessed by a spectrophotometer at 490 nm.

Flow cytometric analysis

Apoptotic cells induced by different concentration LPS were analyzed by an Annexin V/ propidium iodide (PI) apoptosis detection kit (Jiancheng Bioengineering Institute, Nanjing, China). Briefly, after harvesting, washing, and resuspending in 500 μL of binding buffer, cells were stained with 5 μL annexin V-FITC and 5 μL PI in the dark for 10 min at room temperature. Cell fluorescence was determined by a FACScan instrument. Cells positive for Annexin V-FITC were considered as apoptosis.

TUNEL assay

TUNEL assay was employed to detect cell apoptosis rate using an EdUTP TUNEL cell detection kit (Ribobio, Gangzhou, China). Briefly, treated hepatocytes were seeded in 96-well plates, fixed in 4% paraformaldehyde, permeabilized with 0.1% Triton X-100, and then incubated with TUNEL solution. Afterwards, nucleus was then labelled with DAPI and the fluorescence-labeled image was visualized by a confocal microscope.

Immunofluorescence

Autophagy was assessed by counting the number of LC3 dots per cell. Treated hepatocytes (2×10^5 cells/well) were seeded onto 6-well plates with sterile glass cover slips, and then transfected with red fluorescent protein LC3 and enhanced green fluorescent protein GFP. After 72 h incubation, washed cells were analyzed by a laser scanning confocal microscope.

Proteasome and autophagy-lysosomal inhibitor assay

Proteasome inhibitor MG132 (#M7449) and autophagy-lysosomal inhibitor chloroquine (CQ, #C6628) were purchased from Sigma. Briefly, 293T cells were maintained in fresh medium supplemented with 1% FBS in the presence or absence of MG132 (10 μM) or CQ (50 μM) for 36 h. The collected cells were then subjected to Western blotting.

Chromatin immunoprecipitation assay (ChIP)

Three potential binding sites between GLI2 and SYVN1 promoter (BS1: -1153/-1147; BS2: -1099/-1088; BS3: -573/-562) were indicated by hTFtarget (<http://bioinfo.life.hust.edu.cn/hTFtarget#!/>). For ChIP assay, cells were starved overnight and cross-linked with 1% (v/v) formaldehyde. After sonicating the chromatin into fragments of 100 to 400 bp and pre-clearing the lysates with A/G beads, 100 μL lysate was immunoprecipitated with 2 μg of the following antibodies: anti-GLI2 (PA1-28838; ThermoFisher Scientific, Carlsbad, USA) or anti-IgG (14678-1-AP; ThermoFisher). After that, washed DNA was reversed cross-linked overnight, and then analyzed by standard PCR.

Dual-luciferase reporter assay

Wild-type luciferase reporter plasmids (SYVN1 WT) containing predicted binding sites with GLI2 and mutant plasmids (SYVN1 MUT) containing mutant binding sites were established by RIBOBIO (Guangzhou, China). Then, 100 ng SYVN1 WT/MUT vectors were transfected into hepatocytes together with 40 nM shNC or shGLI2 using Lipofectamine 3000. After 48 h, the cells were treated with LPS (5 $\mu\text{g}/\text{mL}$) for 6 h. Finally, cells were lysed and the luciferase activity was measured using a Dual-Luciferase reporter system.

RNA pull-down

After transcribing and end-labeling with desthiobiotin, RNAs were incubated with protein lysates, followed by binding to Streptavidin Magnetic Beads lysates. Next, lysate was incubated for 2 h at 4°C with rotation in 100 μL \times RNA-protein binding buffer containing 100 μg total

protein. After washing, complexes were isolated from streptavidin Magnetic Beads. RNA-binding-protein was assessed in the pull-down by Western blotting.

RNA immunoprecipitation (RIP)

After cross-linking with formaldehyde, cells were harvested, resuspended, and centrifugated to obtain nuclei. Then, cells were resuspended in RIP buffer, supplemented with protease and RNase inhibitors, followed by incubating with magnetic beads conjugated with anti-IGF2BP3 (MA5-27481, ThermoFisher) or IgG overnight with rotation. RNA was eluted in RIP elution buffer and then extracted and enriched.

Co-immunoprecipitation (Co-IP)

The extract from 293T cell transfected with SFB (S-protein/Flag/streptavidin-binding peptide)-tagged SYVN1, Myc-tagged PPAR α , HA-Ubiquitin-WT, HA-tagged ubiquitin K48 or K48R, or HA-tagged ubiquitin K63 or K63R plasmids was used to perform Co-IP assay. At 48 h post-transfection, cells were lysed with IP lysis buffer (Pierce), and incubated with S-protein agarose (Millipore, Billerica, MA, USA) at 4°C overnight. Primary hepatocytes were treated with anti-SYVN1 or anti-PPAR α for 12 h and then harvested in RIPA cell lysis buffer. After centrifugating at 12000 g for 25 min, a portion of the supernatant was collected as an input as input, and the rest of cell lysate for incubation with following antibodies: anti-Flag (#2044; Cell Signaling Technology, MA, USA), anti-SYVN1 (13473-1-AP, ThermoFisher), anti-Myc (M4439; Sigma Aldrich, St. Louis, MO, USA), anti-PPAR α (MA5-37652, ThermoFisher) overnight at 4°C. Immune complexes were isolated by protein A/G beads. Coimmunoprecipitates were resolved by SDS-PAGE and measured by Western blotting as described below. For detecting the ubiquitinated degradation of PPAR α , immunoprecipitation of pulled down samples with anti-HA (ubiquitin, ab9110, Abcam) were used to observe bands of polyubiquitinated PPAR α .

Measurement of alanine transaminase (ALT) and aspartate transaminase (AST)

To determine the liver injury of mice, we collected mouse blood, and then the blood was centrifuged at 4000 rpm for 10 min to obtain the serum. ALT and AST in the serum were determined by respective kits (Jiancheng Bioengineering Institute, Nanjing, China).

Histopathological examination

Liver tissues were fixed in 4% paraformaldehyde and buried by paraffin bag. 5 μ m sections were cut from tissues and then stained with hematoxylin and eosin (H&E). After that, sections were photographed by a microscope (Nikon, Japan). Liver injury was evaluated by an injury grading score (Grade 1-4).

Immunohistochemistry (IHC)

Slices of liver tissues were subjected to antigen retrieval by heating in a microwave oven in 10 mmol/L citrate buffer for 3 min. Then, sections were incubated with primary antibodies against LC3B (ab192890, Abcam, Cambridge, MA, USA), PPAR α (MA5-37652, ThermoFisher), SYVN1 (13473-1-AP, ThermoFisher), GLI2 (PA1-28838, ThermoFisher), and IGF2BP3 (MA5-27481, ThermoFisher). After incubating with poly-peroxidase-anti-mouse/rabbit IgG, immunohistochemical reaction was visualized through staining with DAB, followed by counterstaining with hematoxylin-based reagents which was subsequently analyzed under a microscope.

Quantitative real-time PCR (RT-qPCR)

Total RNAs were extracted with Trizol reagent (Invitrogen) following the manufacturer's instructions, and then was reverse-transcribed to cDNA with Prime-Script RT-PCR master mix (Takara, Tokyo, Japan). RT-qPCR process was performed with SYBR Green qPCR (Applied Biosystems, Carlsbad, CA, USA; 4309155). GAPDH was regarded as the internal control. The gene expression levels were presented as fold changes relative to the expression levels of appropriate controls using the $2^{-\Delta\Delta C_t}$ method. The primers were provided in [Table S2](#).

Western blot analysis

Proteins were extracted from cells and tissues, and the concentration was quantified. Typical SDS (10%)-polyacrylamide gels was utilized to purify the proteins (~50 μ g) extracted from every group. Afterwards, the purified proteins were transferred to a polyvinylidene difluoride (PVDF) membrane. Placed the membrane into a petri dish containing 5% milk for 1 h to block non-specific sites. Discarded the milk and rinse the membranes and dish three times with PBS, then added the PBS containing primary antibodies into the dish. After overnight incubation, rinse the membrane and dish again three times with PBS, then added horseradish peroxidase-conjugated secondary antibody (sc 2004, Santa Cruz Biotechnology) and incubated for 1 h. The antibody-reactive bands were detected with ECL reagent (Millipore, Billerica, MA, USA). β -action (ab8226, Abcam) was used as an internal control. The following primary antibodies were used: anti-GLI2 (PA1-28838, ThermoFisher), anti-PPAR α (MA5-37652, ThermoFisher), anti-TFEB (ab264421, Abcam), anti-LC3-II/I (ab128025, Abcam), anti-p62 (ab109012, Abcam), anti-Beclin-1 (ab302669, Abcam), anti-AMPK α (ab32047, Abcam), anti-p-AMPK α (ab133448, Abcam), anti-mTOR (ab32028, Abcam), anti-p-mTOR (ab109268, Abcam), anti-MDM2 (ab259265, Abcam), anti-STUB1 (ab134064, Abcam), anti-NEDD4L (MA5-32294, ThermoFisher), anti-RANBP2 (PA1-4995, ThermoFisher), anti-UBE4B (ab126759, Abcam), anti-SYVN1(13473-1-AP, ThermoFisher), anti-BARD1 (ab226854, Abcam), anti-CBLC (PA5-87032, ThermoFisher), and anti-IGF2BP3 (MA5-27481, ThermoFisher). Antibodies were also showed in [Table S3](#).

QUANTIFICATION AND STATISTICAL ANALYSIS

Data are expressed as the mean \pm SD. SPSS 24.0 was used for statistical analysis. Differences in the overall survival (OS) were estimated and compared by the Kaplan–Meier method. Student’s t-test was performed to evaluate the differences between two groups; one-way ANOVA was performed to determine significant differences between multiple groups. *P* value lower than 0.05 was considered as statistically significant.